# Near-self-imaging cavity for three-mode optoacoustic parametric amplifiers using silicon microresonators

Jian Liu,[1,2,7] F. A. Torres,[2,8] Yubo Ma,[1,2] C. Zhao,[2] L. Ju,[2] D. G. Blair,[2] S. Chao,[3] I. Roch-Jeune,[4] R. Flaminio,[5] C. Michel,[5] and K.-Y. Liu[6]

[1]Department of Astronomy, Beijing Normal University, Beijing 100875, China

[2]School of Physics, University of Western Australia, 35 Stirling Highway, Crawley, Western Australia 6009, Australia

[3]Institute of Photonics Technologies and E. E. Department, National Tsing Hua University, 101 Kuangfu Rd. Sec. 2, Hsinchu 300, Taiwan

[4]IEMN UMR CNRS 8520, av Poincaré, BP 60069, 50652 Villeneuve d'Ascq Cedex, France

[5]Laboratoire des Matériaux Avancés (LMA), IN2P3/CNRS, Université de Lyon, F-69622 Villeurbanne, Lyon, France

[6]Australian National Fabrication Facility (Queensland Node), Australian Institute for Bioengineering and Nanotechnology, The University of Queensland, Brisbane, QLD 4072, Australia

[7]e-mail: Jianliu@mail.bnu.edu.cn

[8]e-mail: Francis.Achilles.Torres@physics.uwa.edu.au

Received 23 October 2013; accepted 11 December 2013;
posted 20 December 2013 (Doc. ID 198405); published 5 February 2014

Three-mode optoacoustic parametric amplifiers (OAPAs), in which a pair of photon modes are strongly coupled to an acoustic mode, provide a general platform for investigating self-cooling, parametric instability and very sensitive transducers. Their realization requires an optical cavity with tunable transverse modes and a high quality-factor mirror resonator. This paper presents the design of a table-top OAPA based on a near-self-imaging cavity design, using a silicon torsional microresonator. The design achieves a tuning coefficient for the optical mode spacing of 2.46 MHz/mm. This allows tuning of the mode spacing between amplification and self-cooling regimes of the OAPA device. Based on demonstrated resonator parameters (frequencies ~400 kHz and quality-factors $\sim 7.5 \times 10^5$) we predict that the OAPA can achieve parametric instability with 1.6 μW of input power and mode cooling by a factor of $1.9 \times 10^4$ with 30 mW of input power. 

*OCIS codes:* (190.4970) Parametric oscillators and amplifiers; (140.0140) Lasers and laser optics.
http://dx.doi.org/10.1364/AO.53.000841

## 1. Introduction

Optoacoustic systems are attracting considerable interest for quantum optomechanics and signal transduction. In such devices, modes of acoustic (or mechanical) resonators are coupled to optical modes through a nonlinearity provided by the radiation pressure force. This coupling provides a tool to study quantum effects at the macroscopic scale and to achieve quantum limited sensitivity in detecting small displacements and weak forces. Laser cooling of acoustic resonators to their quantum ground state has been achieved in experiments with sufficient optoacoustic coupling [1–4], and extremely high sensitivity transducers have been demonstrated [5–10].

Optoacoustic interactions represent a macroscopic form of Brillouin scattering [11] in which electrostriction couples optical fields and acoustic waves. A travelling electromagnetic wave scatters from a moving

1559-128X/14/050841-09$15.00/0

sound grating in a bulk medium (phonon frequencies up to THz), producing a second electromagnetic wave. In the case of optoacoustic interactions, an optical field scatters on the surface of a vibrating mirror (phonons in the MHz range).

When considering optoacoustic interactions in an optical cavity, it is important to distinguish between two- and three-mode interactions. In a two-mode interaction, an acoustic mode scatters an input beam to create a pair of sidebands within the bandwidth of the same cavity mode. Depending on side-band asymmetry, this can lead to suppression of the acoustic mode (self-cooling [12,13]) or amplification of the acoustic mode. Four frequencies are present, but supported by two modes–one acoustic and one optical.

In a three-mode interaction, an input beam and scattered beam are in different cavity transverse modes. Two optical modes and one acoustic mode are involved. This interaction is analogous to a photonic molecule [14] and is a tuned system that allows the creation of quantum-optical acoustic amplifiers capable of free oscillation (phonon lasers [15]), mode cooling, and amplification of small signals.

Three-mode interactions are qualitatively and quantitatively different from two-mode interactions since power flows at three frequencies. In appropriately designed systems, the optoacoustic coupling can be much greater as it depends on the product of three, high quality-factors (two optical and one acoustic). We will show here that a practical three-mode optoacoustic parametric amplifier (OAPA) can achieve very high self-cooling factors $\sim 10^4$, compared with cooling factors ~30 achieved with two-mode self-cooling [3,4,16].

Braginsky *et al.* first predicted three-mode optoacoustic parametric interactions [17,18] in the context of long-baseline laser-interferometer gravitational wave detectors [19]. This analysis was extended to three dimensions [20] including detailed modeling of acoustic and optical mode structures by Zhao *et al.*, while Ju *et al.* showed that multiple mode interactions could contribute to parametric gain [21].

The theory was confirmed by Evans *et al.* [22], while Zhao and co-workers [5,23] have confirmed the detailed physics of three-mode interactions in long Fabry–Perot cavities. Zhao *et al.* observed these interactions in an 80 m cavity [5] and recently reported the first demonstration of ultrasonic acoustic modes driven by radiation pressure using three-mode parametric interactions [23].

Three-mode interactions have been observed in solid state resonator structures [24] and recently, the first tunable free space three-mode interaction system was demonstrated using a 50 nm thick membrane between two mirrors [25].

A crucial requirement of three-mode interactions is a high quality-factor acoustic resonator that scatters light into a cavity transverse mode with an acoustic mode frequency that matches the frequency gap between both cavity modes. The high quality-factor is required to reduce thermal noise and to increase the parametric gain $R$, a dimensionless quantity which describes the strength of the optoacoustic interaction relative to the losses of the acoustic resonator.

Assuming that the three-mode system is tuned such that $\omega_m = \omega_0 - \omega_1$, where $\omega_0$, $\omega_1$, and $\omega_m$ are the optical carrier mode, high-order mode and acoustic mode frequencies, respectively, the parametric gain $R$ is given by the following formula [17,26]:

$$R = \frac{8 I_{\text{in}} Q_0 Q_1 Q_m \Lambda}{m L^2 \omega_0 \omega_m^2}, \tag{1}$$

where $I_{\text{in}}$ is the input power, $Q_0$ and $Q_1$ are quality-factors of the cavity modes, $Q_m$ is the quality-factor of the acoustic mode, $m$ is the effective mass of the resonator, and $L$ is the cavity length. The overlap factor $\Lambda$ [17,21] between the $\text{TEM}_{00}$, $\text{TEM}_{01}$, and the acoustic mode shapes determines the strength of three-mode interactions. It is an integral of the product of the three-mode shapes. The magnitude of $\Lambda$ depends on the alignment and the relative sizes of the optical and acoustic modes. Thus, to ensure a suitable overlap factor, it is important to optimize the beam spot sizes and alignment, in relation to the resonator structure.

This paper presents the design and predicted performance of a practical OAPA device developed from the concept first presented in [26]. We present the design and validation studies of a compact tunable OAPA system based on a Fabry–Perot [27] cavity with a high quality-factor mg-scale silicon microresonator [28] as an end mirror. This could also provide a platform for studying parametric instability, an important issue in advanced gravitational-wave detectors [19].

The torsional acoustic vibration of a flat mirror is an effective means for obtaining a large spatial overlap between $\text{TEM}_{00}$, $\text{TEM}_{01}$ optical modes, and the acoustic mode. Our design matches the acoustic resonator dimensions to the spot sizes for a $\text{TEM}_{00}$ pump mode and a $\text{TEM}_{01}$ high-order mode. The torsion mode frequency near 400 kHz dictates the requirement for the optical mode gap for a reasonable cavity size.

OAPAs can be operated in two regimes: (a) cooling and (b) amplification and self-sustained oscillation. The design presented here is based on a three-element near-self-imaging (NSI) cavity, which allows beam spot-size optimization and tuning of the optical-mode gap by a few MHz, sufficient to span the two operating regimes.

This paper is organized as follows: In Section 2, we present the design and properties of a suitable high quality-factor resonator with optical coatings. In Section 3, we present the NSI cavity design that allows cooling, amplification, and parametric instability to be achieved. In Section 4, we predict the performance of the OAPA, which is limited by radiation

damage and thermal dissipation if operated at cryogenic temperatures.

### 2. Silicon Resonator with Optical Coatings

The long standing problem of the acoustic loss of multilayer optical coatings [29,30] restricts the options for the design of high quality-factor optical microresonators. To minimize acoustic losses, the resonator is designed to reduce the elastic strain in the optical coatings by applying them only on a central element, designed to move as a rigid body in a torsion motion. In the future, this design could also allow an inductive sensor loop to be attached without incurring large acoustic losses.

The resonator design is illustrated in Fig. 1. Resonators consist of three paddles, inspired by previous work [31], connected by torsion rods, fabricated on 20 mm by 20 mm standard silicon wafers. The paddle design consists of a 1 mm by 1 mm central paddle supported by two isolation paddles (1 mm by 1.8 mm). The torsion rods have length of 0.5 mm and width of 0.3 mm. Wafer thickness of 365, ~500, and 670 μm were used. For the design presented here, we will focus on a resonator with observed frequency 401.5 kHz and thickness 515 μm [28].

The finite element modeling (FEM) software ANSYS 14.0 was used to develop the torsion resonator, with approximately 140 000 nodes to represent the resonator, a mesh size of 300 μm on the frame, and a finer mesh size of 50 μm on the paddles and torsion rods. The resonator was modeled to determine the amplitude distribution of acoustic modes and to ensure that torsion modes were separated in frequency from resonances of the frame. The modes of interest [see Fig. 1(c)] should have strain energy localized on the torsion rods and low energy in the frame. Such modes were expected to have a good isolation from suspension losses. Localization of the strain energy in the torsion rod segments holding the middle paddle, and minimal strain energy on the paddle itself, confirmed the near rigid body behavior of the central paddle.

Resonators for this OAPA system have been fabricated at the Institute of Photonics Technologies of the National Tsing Hua University in Taiwan, at the Institute of Electronic, Micro-electronic and Nanotechnology, the Société Européenne de Systèmes Optiques, and the Laboratoires de Matériaux Avancés, in France, and at the Australian National Fabrication Facility Ltd. in Queensland.

Following careful dimension measurements of resonators fabricated by dry etching [32] or laser micromachining [33], we used FEM modeling to help identify the torsion modes of interest. The 401.5 kHz mode was consistent with the predicted torsion mode frequency for the resonators fabricated from monocrystal (100) boron-doped silicon with thickness of $500 \pm 25$ μm.

Thin film optical coatings were applied on 365 μm thickness resonators as a test of the coating technique, within a square area of 800 μm by 800 μm, center on the middle paddle. The coatings consisted of 14 alternating layers of $SiO_2$ and $Ta_2O_5$ with total thickness 5.0 μm. The specified reflectivity was 99.997% [29,30], at 1064 nm. Future resonators will use higher reflectivity coatings and thicker wafers. This coated paddle is intended as the end mirror in the NSI cavity design presented in the next section.

FEM modeling was used to estimate the losses from coatings by calculating the ratio of the strain energy stored in the coatings $\Delta E$, and the total strain energy $E$ of the acoustic mode. In the absence of suspension losses, the acoustic quality-factor can be approximated by [21] $Q_m^{-1} = Q_i^{-1} + Q_c^{-1}(\Delta E/E)$, where $Q_i$ and $Q_c$ are the intrinsic and coating quality-factors. For coatings on the 401.5 kHz resonator, the calculated energy ratio is $1.7 \times 10^{-3}$. Assuming a typical coating loss [29] of $Q_c^{-1} = 2.5 \times 10^{-4}$, we expect to achieve $Q_m \sim 1.9 \times 10^6$ if $Q_i = 10^7$, and $Q_m \sim 7.0 \times 10^5$ if $Q_i = 10^6$. There is some uncertainty on the intrinsic quality-factor of thin wafers, due to the contribution of surface losses [34].

The acoustic loss contribution from the coatings is very sensitive to the wafer thickness. This loss

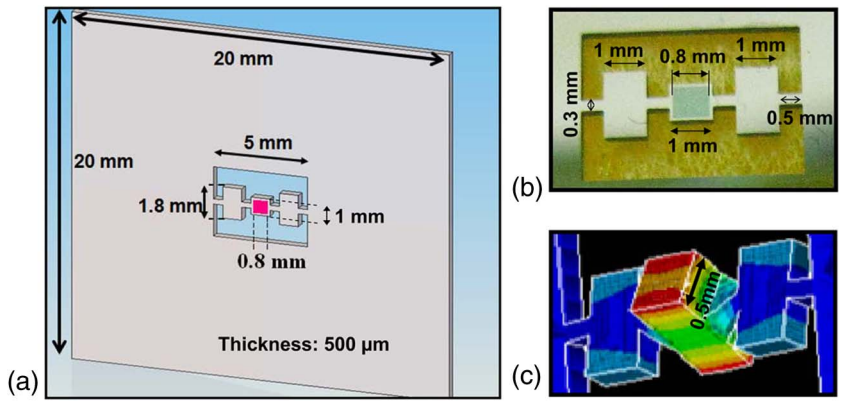


Fig. 1. Micromechanical silicon resonator with optical coating. (a) Dimensions: 20 mm by 20 mm frame, of thickness 500 μm, and three paddles (1 mm wide). The central paddle contains a 0.8 mm square 14-layer tantala/silica optical coating (total thickness ~5.0 μm). (b) Photograph showing paddles and central coating. (c) Finite element modeling (FEM) projection of the torsion mode of interest in which the central paddle has maximum amplitude, shown by the contour plot of deformation.

contribution could be considerably reduced using small changes to the coating area and substrate thickness.

While the intrinsic quality-factor of bulk silicon and thin silicon flexures has been observed to be very high [34,35], the quality-factor of wafers is uncertain because it is difficult to distinguish between suspension losses and intrinsic losses. As stated by Chandorkar *et al.* [36], the heat generation in the resonator due to deformation is negligible for a pure torsion mode. For this reason, thermoelastic loss can be ignored.

We measured the mode frequencies and quality-factors of resonators without coating using an optical lever and piezo excitation system [28]. Quality-factors in the range $5.0 \times 10^5$–$8.6 \times 10^5$ were observed, reasonably close to our design goal.

We also observed that the quality-factor depends greatly on the position of the wafer holder, indicating that suspension losses are not negligible. A comparison of resonators will be published elsewhere.

### 3. Cavity Design

An OAPA requires a cavity design that is well matched to the acoustic resonator. Here we present a three-element NSI optical cavity design that meets the requirements to achieve appropriate optical-mode frequencies and spot size to enable strong three-mode optoacoustic parametric interactions in a compact tabletop system.

In a single optical cavity, for a given cavity length $L$, the resonant frequency of the $\mathrm{TEM}_{mn}$ mode is given by

$$\nu = \frac{c}{2L}\left[p + \frac{\alpha}{\pi}(m + n + 1)\right], \tag{2}$$

where $c$ is the speed of light, $p$ is the longitudinal mode index, $m$ and $n$ are transversal indexes, and $\alpha$ is the Gouy phase shift of the $\mathrm{TEM}_{00}$ mode over one cavity length. If $\alpha = k\pi$, where $k$ is an integer, the cavity is fully degenerate, and all $\mathrm{TEM}_{mn}$ modes and their linear combinations resonate simultaneously. This is a self-imaging cavity [37]. Similar cavities have been studied and used in multi-mode squeezing experiments [38].

The configuration of a self-imaging cavity is fixed after choosing the mirror radius of curvature $R_0$ and the lens focal length $f$. The spacing between components is given by

$$L_1 + L_2 = f + R_0, \tag{3}$$

and

$$L_3 = f + f^2/R_0. \tag{4}$$

A small adjustment to the position of any component in the self-imaging cavity breaks the degeneracy, thereby creating the NSI cavity, in which there is a small tunable frequency gap between modes.

As stated in the Introduction, the 400 kHz acoustic frequency of the torsional microresonator should match the frequency gap between the $\mathrm{TEM}_{00}$ and $\mathrm{TEM}_{01}$ modes in our cavity design. The $\mathrm{TEM}_{01}$ mode is chosen for its suitable spatial overlap with the torsional acoustic mode of the resonator.

Another requirement of the OAPA is that the optical mode size should match the size of the acoustic mode. For a simple two-mirror optical cavity, a mode gap near 400 kHz is easy to achieve in a near-planar or a near-concentric cavity [39], but it is difficult to achieve the correct mode size in a small cavity. This is easier in a three-element NSI cavity, using small adjustments of the position of $L_T$ (see Fig. 2) to adjust both the mode gap and the mode size.

As shown in Eq. (2), the mode gap between the $\mathrm{TEM}_{00}$ mode and the $\mathrm{TEM}_{01}$ mode is determined by the Gouy phase shift $\alpha$, which is a function of the cavity length $L$, and therefore of the radius of curvature $R_0$ of mirror $M_0$ and the focal length $f$ of the lens $L_T$.

Here we will derive the Gouy phase shift and the optimal positions of the components in the cavity in order to produce three-mode interactions. To simplify the analysis, the cavity is divided into three parts: $L_1$, $L_2$, and $L_3$. We use $\phi_1$ for the Gouy phase shift from $M_0$ to the waist $W_1$, $\phi_2$ for the phase shift from the waist $W_1$ to the lens $L_T$, and $\phi_3$ for the phase shift from the lens $L_T$ to the resonator $M_1$. The total Gouy phase shift in the cavity is then

$$\alpha = \phi_1 + \phi_2 + \phi_3. \tag{5}$$

For a Gaussian beam, the Gouy phase shift at any point is given by

$$\phi = \arctan(z/z_R), \tag{6}$$

where $z$ is the displacement of the point relative to the waist, $z_R$ is the Rayleigh range given by $z_R = \pi W_i^2/\lambda$, where $\lambda$ is the laser wavelength, and $W_i$ is either the waist before ($i = 1$) or after ($i = 2$) the lens $L_T$.

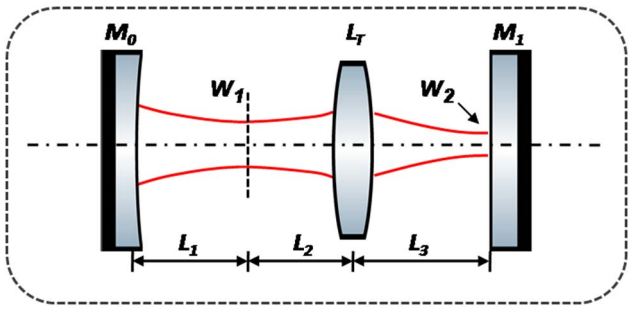


Fig. 2. NSI optical-cavity concept and key parameters. A torsional microresonator ($M_1$) interacts with the $\mathrm{TEM}_{00}$ mode and the $\mathrm{TEM}_{01}$ mode. We can continuously change the mode gap between the two optical modes by tuning the position of the lens $L_T$. $W_1$ and $W_2$ are the waist sizes before and after the lens $L_T$, respectively. In a practical cavity, the tuning lens $L_T$ is replaced with a tuning mirror $M_T$ (shown later in Fig. 4).

In the NSI cavity, the laser spot size on the resonator is waist $W_2$, which must be tailored to fit within the square mm surface of the torsional resonator. The distance $L_3$ between the resonator $M_1$ and the lens $L_T$ must satisfy

$$\phi_3 = \arctan\left(\frac{L_3}{z_R}\right), \tag{7}$$

where $z_R = \pi W_2^2/\lambda$ is the Rayleigh range after the lens.

The properties of the laser beam after passing through the lens are completely determined by the state of the beam before the lens and the transmission matrix of the lens. The waist position $L_2$ of the first waist, and the waist size $W_1$ can be derived directly from the ray transfer relation of a Gaussian beam, given by

$$q' = \frac{fq}{f-q}, \tag{8}$$

where $f$ is the focal length of $L_T$, $q$ is the complex parameter of a Gaussian beam defined by $q = z + iz_R$, and $q'$ is the complex parameter before the lens. From Eq. (8) we obtain $L_2$ and $W_1$:

$$L_2 = f + \frac{(L_3 - f)f^2}{(L_3 - f)^2 + z_R^2}, \tag{9}$$

$$W_1 = \frac{f^2 W_2^2}{(L_3 - f)^2 + z_R^2}. \tag{10}$$

With the values of $L_2$ and $W_1$ determined, phase shift $\phi_2$ is given by

$$\phi_2 = \arctan\left(\frac{L_2}{z'_R}\right), \tag{11}$$

where $z'_R$ is the Rayleigh range before the lens, given by

$$z'_R = \frac{\pi W_1^2}{\lambda}. \tag{12}$$

The radius of curvature $R_0$ of the mirror $M_0$, and the waist size $W_1$ are related to $L_1$ as follows:

$$R_0 = L_1\left(1 + \left(\frac{\pi W_1^2}{\lambda L_1}\right)^2\right). \tag{13}$$

From $L_1$ we obtain $\phi_1$:

$$\phi_1 = \arctan\left(\frac{L_1}{z'_R}\right). \tag{14}$$

Equations (7), (11), and (14) show that the Gouy phase shift over the cavity length is determined by four parameters: $W_2, R_0, f$, and $L_3$. We chose the size of $W_2$ to balance two requirements: (1) high overlap between the optical and acoustic modes; (2) low optical diffraction loss to maintain a high cavity finesse. Considering the resonator size of 1 mm by 1 mm, a 0.2 mm beam waist was chosen to have an overlap factor of 0.1 and a diffraction loss of 15 ppm. If we fix $R_0$ and $f$ by using specific components, the Gouy phase shift will depend only on $L_3$. Thus, by changing $L_3$, we control the mode gap between optical modes $\mathrm{TEM}_{00}$ and $\mathrm{TEM}_{01}$. Using Eq. (2), we obtain a relationship between the mode gap $\Delta\nu$ and $L_3$ as follows:

$$\Delta\nu = \frac{c}{2\pi(L_1 + L_2 + L_3)}(\phi_1 + \phi_2 + \phi_3 - k\pi). \tag{15}$$

Here $k$ is an integer that indicates the difference in the longitudinal mode index of the two optical modes ($k = 1$ in our case). We have considered different cavity configurations ($R_0$ and $f$ values) to achieve a mode gap of $\Delta\nu = \pm 400$ kHz. We found that a configuration with $R_0 = 50$ mm and $f = 50$ mm is suitable, as we only need to adjust the position of the lens by 325 μm (the tuning gap) to adjust the cavity from amplification to cooling regimes.

For a self-imaging cavity, in which $L_3 = f + f^2/R_0$ [Eq. (4)], using $R_0 = 50$ mm and $f = 50$ mm gives a value of the distance $L_3 = 100.0$ mm. This corresponds to the NSI average value of $L_3$ for instability and cooling regimes, which is 100.16 and 99.84 mm, respectively. This indicates that the tuning of the lens $L_T$ in the cavity is symmetric around the self-imaging point ($\Delta\nu = 0$).

Cavity tuning is demonstrated in Fig. 3 where the mode gap is plotted as a function of the position of the lens relative to the resonator. A tuning coefficient of 2.46 MHz/mm is achieved. When $L_3$ is reduced below 100 mm, the OAPA enters the cooling regime. When $L_3$ is increased above 100 mm, it enters the positive gain regime.

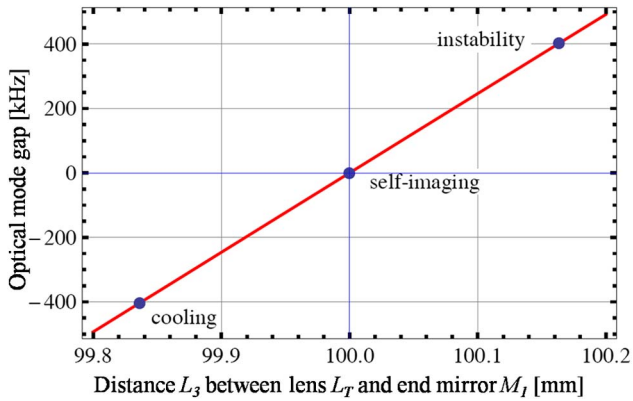


Fig. 3. Mode gap as a function of the position of the micromechanical resonator relative to the lens, with fixed parameters of the radius of curvature and focal length, $R_0 = 50$ mm and $f = 50$ mm. The tuning gap is 325 μm and the tuning coefficient is 2.46 MHz/mm. The tuning is almost linear and symmetric around the self-imaging point.

## 4. Predicted Performance of a Practical NSI Cavity Setup

Based on the design given in the previous sections, we present here a practical experimental setup and performance estimates for a three-mode OAPA shown in Fig. 4. Rather than using a lens as shown in Fig. 2, a practical OAPA uses a mirror to replace the tuning lens. The pump beam requires a pre-mode cleaner (PMC) to insure that the injection is a pure $TEM_{00}$ mode, and must be mode matched and frequency locked using a standard Pound–Drever–Hall (PDH) locking scheme [40].

The NSI cavity needs to be operated in a vacuum to achieve high acoustic-resonator quality-factors and to be sufficiently rigid to maintain dimensional constraints. Piezo mirror mounts for the input mirror and the tuning mirror can allow the required tuning range. Experience with a membrane cavity three-mode interaction setup [25] has demonstrated the importance of alignment and tuning to achieve maximal overlap between the acoustic mode and $TEM_{01}$ mode.

As shown in Fig. 4, a quadrant photodetector can be used in common mode for the PDH locking, and in differential mode to monitor the OAPA signal at 400 kHz. This signal is a beat frequency between the $TEM_{00}$ and $TEM_{01}$ modes, which is proportional to the amplitude of the torsional resonator. In the absence of external excitation, the quadrant photodetector output should record a thermally driven acoustic mode amplitude of the torsional resonator. At low input power, this signal should represent the kT thermal energy of the resonator, but as power increases, the mode should be amplified or suppressed, as discussed further below.

To predict the performance of the OAPA described here, we need to determine the maximum power the device will withstand. This depends on two factors: optical damage and thermal heating. Using the continuous wave damage threshold for thin-film optical coatings, ~1 MW/cm$^2$ for currently available technologies [29], and the designed waist size at $M_1$ of 0.2 mm, the circulating power limit is ~1.2 kW.

The transmissivity and absorption of the resonator coatings will allow some of the circulating power to be absorbed by the silicon substrate, which could alter the acoustic torsional-mode frequency and detune the NSI cavity.

The input mirror is designed for a transmissivity of $10^{-4}$. Combined with the 1 ppm loss of the coatings and 15 ppm diffraction loss of the resonator reflective coating, the OAPA cavity can achieve a finesse of $6.3 \times 10^4$, calculated from the relationship: $F = 2\pi/\phi$, where $F$ is the finesse, and $\phi$ is the total loss. The circulating power limit sets the input power limit to 30 mW.

Only a small fraction of the input power needs to be dissipated by the resonator. Since the silicon substrate will strongly absorb 1064 nm light, the power absorbed by the resonator will be the sum of the coating transmissivity and absorption. Assuming 1 ppm transmission, coating absorption of 0.25 ppm, and silicon absorption of 0.5, a maximum of ~1 mW should be absorbed by the resonator. As discussed below, this could be reduced in resonators designed for cryogenic operations.

We modeled the resonators using the thermal conductivity of 148 W/mK [41] to predict the effects of laser heating. The small mass of the resonator structure and the large thermal conductivity of silicon ensures that the resonator has a short thermal relaxation time (~ms) to the wafer substrate. Thereafter it cools by blackbody radiation.

At room temperature, the 1 mW from laser heating is estimated to cause the wafer temperature to rise by 3.2 K before equilibrium is reached with dissipation from blackbody radiation. The blackbody radiation thermal relaxation time for the wafer is ~10 minutes.

We used the temperature dependence of the Young's modulus Y(T) of silicon to confirm the above analysis, as changes to the Young's modulus are the

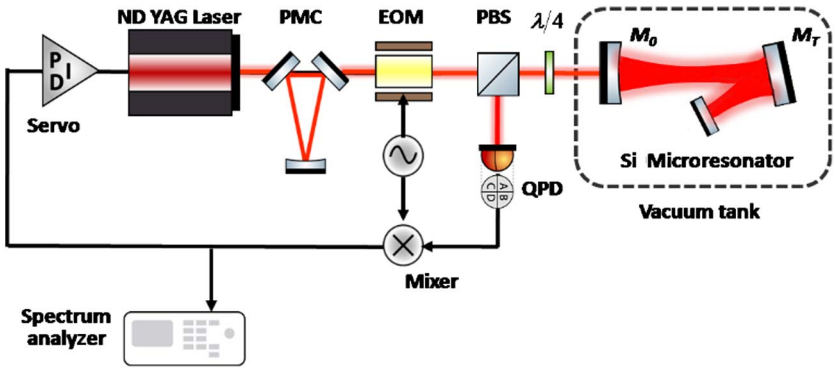


Fig. 4. Experimental setup of the NSI cavity for three-mode interactions. The laser light passes through a PMC to clean up high-order modes, and is then phase modulated by an electro-optic modulator (EOM) for PDH locking of the laser frequency to the NSI cavity. A 400 kHz torsional microresonator acts as the end mirror of the NSI cavity, which interacts with the cavity $TEM_{00}$ and $TEM_{01}$ modes. The sum signal from the quadrant photodetector is used for PDH locking while its differential signal is used to monitor the resonator amplitude. The mode gap between the two optical modes is adjusted by tuning the position of $M_T$.

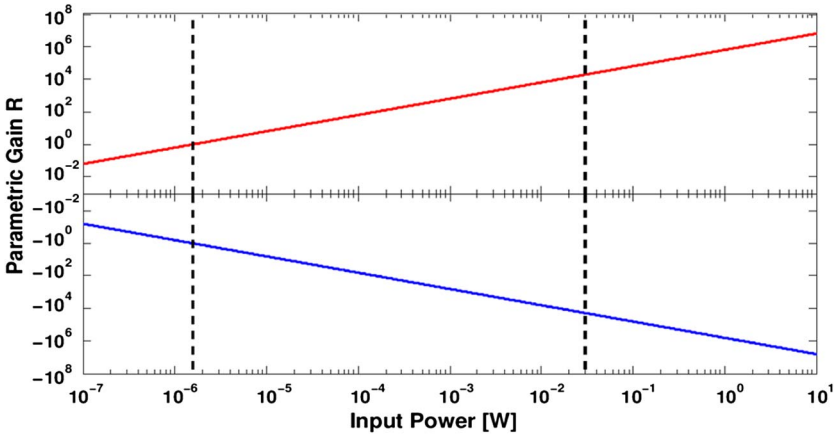


Fig. 5. Expected parametric gain for given laser input power values. Parametric instability (gain $R = 1$) is achieved with 1.6 μW (left vertical–dotted line). The red curve is the achievable acoustic mode amplification and instability (for $R \geq 1$), and the blue curve is mode cooling. Our system allows for 30 mW of input power before the damage threshold of optical coatings is reached. With 30 mW of input power, a cooling factor $\sim 1.9 \times 10^4$ is reached (right vertical–dotted line).

dominating cause of acoustic mode frequency drift [42,43]. The near-linear relation [41] $\Delta Y(T)/\Delta T \approx -7$ MPa/K allows the mode frequency to be used as a temperature probe.

With the low-power laser used in the optical lever for measuring acoustic modes, we could apply known amounts of heat and measure the resonator temperature changes over time. Results were consistent with the simple modeling, above, leading to an expectation that, at maximum optical power, the mode frequency would drift by ~32 Hz due to laser heating. This is small compared with the optical-mode linewidths, so should not vary the OAPA gain.

Two parameters can be used to characterize OAPA performance: (a) power required to achieve parametric instability ($R = +1$) and (b) maximum possible cooling factor. Here we will estimate these factors.

The effective acoustic mode temperature $T_{\text{eff}}$ reached by self-cooling (anti-Stokes mode) is related to the parametric gain $R$ [see Eq. (1)], as shown in Eq. (16) [26]:

$$T_{\text{eff}} = \frac{T_0}{1 - R}, \tag{16}$$

where $T_0$ is the thermodynamic temperature of the acoustic mode.

According to Eq. (16), if $R = +1$, $T_{\text{eff}} \to \infty$, corresponding to parametric instability. Large negative values of $R$ cause strong cooling.

Using Eq. (1) and the parameters reported above, the OAPA achieves $R = 1$ with an incident power ~1.6 μW (cavity finesse of $6.3 \times 10^4$, $Q_0 = Q_1 = 1.3 \times 10^{10}$, and $\Lambda = 0.1$, resonator effective mass $m = 1.17$ mg, and experimentally observed [28] $Q_m = 7.5 \times 10^5$). Figure 5 shows the predicted parametric gain as a function of input power.

Using the maximum input power of 30 mW, and the parameters given above, the maximum cooling gain is $-1.9 \times 10^4$. This gain would allow the resonator effective temperature to be cooled from 300 K to ~15 mK. If the resonator was cryogenically cooled to 76 mK, it would allow self-cooling of the macroscopic resonator acoustic mode to the quantum ground state, near 4 μK [26] [Eq. (16)].

## 5. Conclusions

A three-element NSI cavity has been shown to allow the creation of a high parametric gain three-mode OAPA in a compact setup. We have presented a configuration that allows tuning between positive and negative gain (from parametric instability to strong cooling) with small relative position adjustments of the optical components. The device can be tuned for different optical mode gaps and mechanical resonator frequencies.

We have predicted that the OAPA design presented here can achieve parametric instability, corresponding to a parametric gain $R = 1$ with 1.6 μW of input power. The maximum self-cooling factor, limited by the optical-coating damage threshold, is $1.9 \times 10^4$ with 30 mW of input power. This cooling gain is sufficient to cool the resonator to the quantum ground state from an initial temperature of 76 mK.

The above estimate does not account for the strong reduction of acoustic losses in silicon at low temperatures. A resonator designed to be cooled to the ground state would require reduced laser heating and reduced loss contributions from the optical coatings. If a quality-factor of $10^7$ was achieved, combined with coating losses ~0.1 ppm, the heat load would fall below 100 μW, and the peak cooling factor would increase, making ground state cooling achievable for this mg scale resonator [44].

An OAPA has many potential applications. Because the resonators have long relaxation times (~s), if cooled to the quantum ground state, they could be used as quantum memory devices. Their mm scale makes them suitable to study macroscopic quantum mechanics on scales larger than many other systems used in macroscopic quantum experiments. They are sources of tripartite entanglement.

As room temperature devices, a simple current loop mounted on the central paddle could enable an OAPA to be operated as a sensitive magnetometer or radio frequency field detector. In the first instance, we plan to test the predictions presented here, and use the device for studying three-mode parametric instability and suppression methods for advanced gravitational wave detectors [19].

We also propose to develop an improved resonator design using silicon-on-insulator wafer technology, to allow a difference in thickness between the frame and the paddles [45]. A design with thin paddles and a thick frame (~mm) will allow simple thermal grounding without incurring suspension losses, which would be necessary for efficient cooling in a very low temperature environment.

This work was supported by the Australian Research Council, the Australian National Fabrication Facility, the French RENATECH network, and Beijing Normal University, for partial funding of the work. We would like to thank Professor Zong-Hong Zhu for making this research possible and Professor Hai-Bo Wang for valuable advice.

## References

1. T. Corbitt, Y. Chen, E. Innerhofer, H. Müller-Ebhardt, D. Ottaway, H. Rehbein, D. Sigg, S. Whitcomb, C. Wipf, and N. Mavalvala, "An all-optical trap for a gram-scale mirror," Phys. Rev. Lett. **98**, 150802 (2007).
2. T. J. Kippenberg, H. Rokhsari, T. Carmon, A. Scherer, and K. J. Vahala, "Analysis of radiation-pressure induced mechanical oscillation of an optical microcavity," Phys. Rev. Lett. **95**, 33901 (2005).
3. S. Gigan, H. R. Böhm, M. Paternostro, F. Blaser, G. Langer, J. B. Hertzberg, K. C. Schwab, D. Bäuerle, M. Aspelmeyer, and A. Zeilinger, "Self-cooling of a micromirror by radiation pressure," Nature **444**, 67–70 (2006).
4. A. Schliesser, P. Delaye, N. Nooshi, K. J. Vahala, and T. J. Kippenberg, "Radiation pressure cooling of a micromechanical oscillator using dynamical backaction," Phys. Rev. Lett. **97**, 243905 (2006).
5. C. Zhao, L. Ju, Y. Fan, S. Gras, B. J. J. Slagmolen, H. Miao, P. Barriga, D. G. Blair, D. J. Hosken, A. F. Brooks, P. J. Veitch, D. Mudge, and J. Munch, "Observation of three-mode parametric interactions in long optical cavities," Phys. Rev. A **78**, 023807 (2008).
6. J. Miller, M. Evans, L. Barsotti, P. Fritschel, M. MacInnis, R. Mittleman, B. Shapiro, J. Soto, and C. Torrie, "Damping parametric instabilities in future gravitational wave detectors by means of electrostatic actuators," Phys. Lett. A **375**, 788–794 (2011).
7. S. P. Vyatchanin, "Parametric oscillatory instability in laser gravitational antennas," Phys. Usp. **55**, 302–305 (2012).
8. S. Forstner, S. Prams, J. Knittel, E. D. van Ooijen, J. D. Swaim, G. I. Harris, A. Szorkovszky, W. P. Bowen, and H. Rubinsztein-Dunlop, "Cavity optomechanical magnetometer," Phys. Rev. Lett. **108**, 120801 (2012).
9. O. Arcizet, P.-F. Cohadon, T. Briant, M. Pinard, A. Heidmann, J.-M. Mackowski, C. Michel, L. Pinard, O. Francais, and L. Rousseau, "High-sensitivity optical monitoring of a micromechanical resonator with a quantum-limited optomechanical sensor," Phys. Rev. Lett. **97**, 133601 (2006).
10. J. M. Dobrindt and T. J. Kippenberg, "Theoretical analysis of mechanical displacement measurement using a multiple cavity mode transducer," Phys. Rev. Lett. **104**, 033901 (2010).
11. G. Bahl, M. Tomes, F. Marquardt, and T. Carmon, "Observation of spontaneous Brillouin cooling," Nat. Phys. **8**, 203–207 (2012).
12. T. J. Kippenberg and K. J. Vahala, "Cavity optomechanics: back-action at the mesoscale," Science **321**, 1172–1176 (2008).
13. P. F. Cohadon, A. Heidmann, and M. Pinard, "Cooling of a mirror by radiation pressure," Phys. Rev. Lett. **83**, 3174–3177 (1999).
14. I. S. Grudinin, H. Lee, O. Painter, and K. J. Vahala, "Phonon laser action in a tunable two-level system," Phys. Rev. Lett. **104**, 083901 (2010).
15. J. B. Khurgin, "Viewpoint: phonon lasers gain a sound foundation," Physics **3**, 16 (2010).
16. O. Arcizet, P.-F. Cohadon, T. Briant, M. Pinard, and A. Heidmann, "Radiation-pressure cooling and optomechanical instability of a micromirror," Nature **444**, 71–74 (2006).
17. V. B. Braginsky, S. E. Strigin, and S. P. Vyatchanin, "Parametric oscillatory instability in Fabry–Perot interferometer," Phys. Lett. A **287**, 331–338 (2001).
18. V. B. Braginsky, S. E. Strigin, and S. P. Vyatchanin, "Analysis of parametric oscillatory instability in power recycled LIGO interferometer," Phys. Lett. A **305**, 111–124 (2002).
19. G. M. Harry, "Advanced LIGO: the next generation of gravitational wave detectors," Class. Quantum Grav. **27**, 084006 (2010).
20. C. Zhao, L. Ju, J. Degallaix, S. Gras, and D. G. Blair, "Parametric instabilities and their control in advanced interferometer gravitational-wave detectors," Phys. Rev. Lett. **94**, 121102 (2005).
21. L. Ju, S. Gras, C. Zhao, J. Degallaix, and D. G. Blair, "Multiple modes contributions to parametric instabilities in advanced laser interferometer gravitational wave detectors," Phys. Lett. A **354**, 360–365 (2006).
22. M. Evans, L. Barsotti, and P. Fritschel, "A general approach to optomechanical parametric instabilities," Phys. Lett. A **374**, 665–671 (2010).
23. C. Blair, S. Susmithan, C. Zhao, F. Qi, L. Ju, and D. Blair, "Radiation pressure excitation of test mass ultrasonic modes via three mode opto-acoustic interactions in a suspended Fabry–Pérot cavity," Phys. Lett. A **377**, 1970–1973 (2013).
24. G. Bahl, J. Zehnpfennig, M. Tomes, and T. Carmon, "Stimulated optomechanical excitation of surface acoustic waves in a microdevice," Nat. Commun. **2**, 403 (2011).
25. X. Chen, C. Zhao, L. Ju, S. Danilishin, D. Blair, H. Wang, and S. P. Vyatchanin, "Observation of three-mode parametric instability," arXiv:1303.4561 (2013).
26. C. Zhao, L. Ju, H. Miao, S. Gras, Y. Fan, and D. G. Blair, "Three-mode optoacoustic parametric amplifier: a tool for macroscopic quantum experiments," Phys. Rev. Lett. **102**, 243902 (2009).
27. S. R. Mallinson, "Fabry–Perot interferometer," U.S. Patent 4,825,262 (25 April 1989).
28. F. A. Torres, P. Meng, L. Ju, C. Zhao, D. G. Blair, K.-Y. Liu, S. Chao, M. Martyniuk, I. Roch-Jeune, R. Flaminio, and C. Michel, "High quality factor mg-scale silicon mechanical resonators for 3-mode optoacoustic parametric amplifiers," J. Appl. Phys. **114**, 014506 (2013).
29. G. M. Harry, M. R. Abernathy, A. E. Becerra-Toledo, H. Armandula, E. Black, K. Dooley, M. Eichenfield, C. Nwabugwu, A. Villar, D. R. M. Crooks, G. Cagnoli, J. Hough, C. R. How, I. MacLaren, P. Murray, S. Reid, S. Rowan, P. H. Sneddon, M. M. Fejer, R. Route, S. D. Penn, P. Ganau, J.-M. Mackowski, C. Michel, L. Pinard, and A. Remillieux, "Titania-doped tantala/silica coatings for gravitational-wave detection," Class. Quantum Grav. **24**, 405–415 (2007).
30. D. T. Wei, "Ion beam interference coating for ultralow optical loss," Appl. Opt. **28**, 2813–2816 (1989).
31. J. P. Davis, D. Vick, D. C. Fortin, J. A. J. Burgess, W. K. Hiebert, and M. R. Freeman, "Nanotorsional resonator torque magnetometry," Appl. Phys. Lett. **96**, 072513 (2010).
32. Y. Mita, M. Kubota, T. Harada, F. Marty, B. Saadany, T. Bourouina, and T. Shibata, "Contour lithography methods for drie fabrication of nanometre–millimetre-scale coexisting microsystems," J. Micromech. Microeng. **16**, S135–S141 (2006).
33. J. Greuters and N. H. Rizvi, "UV laser micromachining of silicon, indium phosphide and lithium niobate for

telecommunications applications," in *OPTO Ireland* (International Society for Optics and Photonics, 2003), pp 479–486.
34. R. Nawrodt, C. Schwarz, S. Kroker, I. W. Martin, R. Bassiri, F. Brückner, L. Cunningham, G. D. Hammond, D. Heinert, J. Hough, T. Käsebier, E.-B. Kley, R. Neubert, S. Reid, S. Rowan, P. Seidel, and A. Tünnermann, "Investigation of mechanical losses of thin silicon flexures at low temperatures," Class. Quantum Grav. **30**, 115008 (2013).
35. R. Nawrodt, A. Zimmer, T. Koettig, C. Schwarz, D. Heinert, M. Hudl, R. Neubert, M. Thürk, S. Nietzsche, W. Vodel, P. Seidel, and A. Tünnermann, "High mechanical Q-factor measurements on silicon bulk samples," J. Phys. **122**, 012008 (2008).
36. S. A. Chandorkar, R. N. Candler, A. Duwel, R. Melamud, M. Agarwal, K. E. Goodson, and T. W. Kenny, "Multimode thermoelastic dissipation," J. Appl. Phys. **105**, 043505 (2009).
37. J. A. Arnaud, "Degenerate optical cavities," Appl. Opt. **8**, 189–195 (1969).
38. B. Chalopin, A. Chiummo, C. Fabre, A. Matre, and N. Treps, "Frequency doubling of low power images using a self-imaging cavity," Opt. Express **18**, 8033–8042 (2010).
39. H. Miao, C. Zhao, L. Ju, S. Gras, P. Barriga, Z. Zhang, and D. G. Blair, "Three-mode optoacoustic parametric interactions with a coupled cavity," Phys. Rev. A **78**, 063809 (2008).
40. R. W. P. Drever, J. L. Hall, F. V. Kowalski, J. Hough, G. M. Ford, A. J. Munley, and H. Ward, "Laser phase and frequency stabilization using an optical resonator," Appl. Phys. B **31**, 97–105 (1983).
41. W. O'Mara, R. B. Herring, and L. P. Hunt, *Handbook of Semiconductor Silicon Technology* (Crest, 2007).
42. S. Reid, G. Cagnoli, D. R. M. Crooks, J. Hough, P. Murray, S. Rowan, M. M. Fejer, R. Route, and S. Zappe, "Mechanical dissipation in silicon flexures," Phys. Lett. A **351**, 205–211 (2006).
43. U. Gysin, S. Rast, P. Ruff, E. Meyer, D. W. Lee, P. Vettiger, and C. Gerber, "Temperature dependence of the force sensitivity of silicon cantilevers," Phys. Rev. B **69**, 045403 (2004).
44. K. Uhlig, "Dry dilution refrigerator with high cooling power," AIP Conf. Proc. **985**, 1287 (2008).
45. E. Serra, A. Borrielli, F. S. Cataliotti, F. Marin, F. Marino, A. Pontin, G. A. Prodi, and M. Bonaldi, "An ultra-low dissipation micro-oscillator for quantum opto-mechanics," Phys. Rev. A **86**, 051801 (2012).